Simultaneous Observation of a Topological Edge State and Exceptional Point in an Open and Non-Hermitian Acoustic System

Weiwei Zhu,[1,2] Xinsheng Fang,[1,2] Dongting Li,[1,2] Yong Sun,[1,2] Yong Li,[1,2,*] Yun Jing,[3,†] and Hong Chen[1,2,‡]
[1]MOE Key Laboratory of Advanced Micro-Structured Materials, School of Physics Science and Engineering, Tongji University, Shanghai 200092, People's Republic of China
[2]Shanghai Key Laboratory of Special Artificial Microstructure Materials and Technology, School of Physics Science and Engineering, Tongji University, Shanghai 200092, People's Republic of China
[3]Department of Mechanical and Aerospace Engineering, North Carolina State University, Raleigh, North Carolina 27695, USA

(Received 24 May 2018; published 20 September 2018)

This Letter reports on the experimental observation of a topologically protected edge state and exceptional point in an open and non-Hermitian (lossy) acoustic system. Although the theoretical underpinning is generic to wave physics, the simulations and experiments are performed for an acoustic system. It has nontrivial topological properties that can be characterized by the Chern number provided that a synthetic dimension is introduced. Unidirectional reflectionless propagation, a hallmark of exceptional points, is unambiguously observed in both simulations and experiments.

DOI: 10.1103/PhysRevLett.121.124501

Introduction.—Exceptional points (EPs), which are branch point singularities associated with the coalescence of eigenvalues and the corresponding eigenvectors, have recently gained substantial attention owing to their intriguing characteristics in parity-time ($\mathcal{PT}$) symmetry systems [1]. A flurry of recent activity has demonstrated extraordinary phenomena associated with the EP in $\mathcal{PT}$ symmetry systems, such as loss induced transparency [2], band merging [3], unidirectional invisibility [4–6], and laser mode selectivity [7,8]. In particular, EPs have been identified in classical wave systems, such as optical [5,7–9], microwave [10], and acoustical systems [11–14]. In fact, EPs can be also observed in other non-Hermitian systems besides the $\mathcal{PT}$ symmetry system. For instance, EPs have been found in passive (lossy) systems [15–24], which can be manifested by a series of features such as unidirectional reflectionless propagation (URP) [22–25].

Meanwhile, topological edge states have grown into a burgeoning research area in condensed matter [26,27] and classical wave physics [28–37]. Topological edge states, or topologically protected edge states, possess the ability of enhancing the field intensity [35] and could give rise to robust one-way propagation [36,38,39]. Although topological properties of non-Hermitian systems have been studied [40–45], topological edge state and EP are largely considered two unrelated topics. This can be possibly attributed to the fact that most topological edge states are obtained in closed and Hermitian systems, whereas EPs are generally harbored in open and non-Hermitian systems. Recently, topological edge states in open systems have been theoretically demonstrated by using one-dimensional resonant photonic crystals with modulated far-field couplings [46]. This provides us the foundation to investigate a variety of open system phenomena pertinent to topological edge states and a possible route for accessing the EP.

In this Letter, we report on the observation of topological edge state and EP in an open system with judiciously tailored losses. Firstly, we obtain topologically protected edge states in a comblike, quasiperiodic acoustic structure with compound unit cells inspired by the commensurate Aubry-Andre-Harper (AAH) model [47–49]. The resulting edge states are locked on one side of the system by a modulated phase. When a critical loss Γ_0 is introduced to the system, the EP is established, giving rise to URP. Interestingly, when the edge state is located in the band gap, a remarkable state can be observed where the reflection is zero for the incident wave from one side and almost unity from the other side. To the best of our knowledge, this is the first experiment to simultaneously achieve the EP and topological edge state. Our work, therefore, builds a nontrivial connection between two seemingly unrelated concepts, i.e., topological edge state and exceptional point.

Model.—Inspired by the AAH model [47–49], a comblike quasiperiodic acoustic structure with compound unit cells composed of Q side-branch tubes (closed-end tubes) attached to a main tube is constructed (Fig. 1). The distance between the nth and $(n+1)$th side-branch tubes in the compound unit cell is modulated as

$$d_n = d\{1 + \delta\cos[2\pi b(n-1) + \phi]\}. \tag{1}$$

Here d is the unmodulated distance, δ represents the strength of cosine modulation, $b = P/Q$ is a rational number with P and Q being two integers with no common

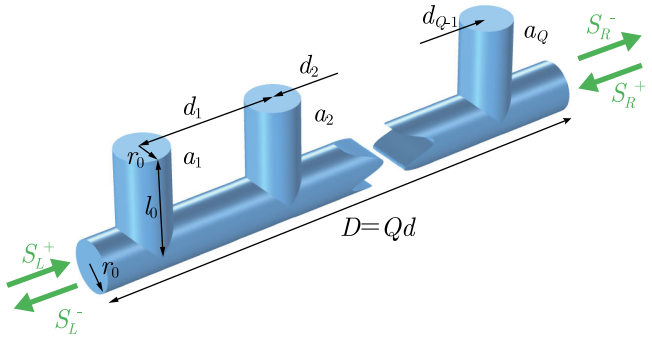

FIG. 1. The schematic of a comblike compound unit cell composed of a main tube (radius r_0) with Q closed-end, side-branch tubes (radius r_0 and length l_0). d_n refers to the distance between the nth and $(n+1)$th side-branch tubes. a_n represents the amplitude of the resonant mode of the nth side-branch tube. The dimensions are $r_0 = 14.5$ mm, $d = 100$ mm, and $l_0 = 58$ mm.

factors, and ϕ defines an arbitrary phase. ϕ has an allowed value ranging from $-\pi$ to π and is the key parameter to relate a one-dimensional system to a two-dimensional topologically nontrivial system that can be characterized by the Chern number [47–49]. The broken time-reversal symmetry is necessary to obtain the nonzero Chern numbers. In our system, the time-reversal symmetry is preserved for the configuration with fixed ϕ. The modulation distance, however, provides an effective gauge magnetic field which breaks the time-reversal symmetry [46].

Because the main tube is of subwavelength size (radius r_0), only the fundamental mode is allowed. The acoustic compound unit cell can be described by the temporal coupled mode equation for the lowest resonant mode amplitudes $\tilde{a}_n = a_n e^{i\omega t}$ of the nth side-branch tube [50],

$$\frac{d}{dt}\tilde{a}_n = (i\omega_0 - \gamma - \Gamma)\tilde{a}_n - \gamma\sum_{n'\neq n}\Lambda_{nn'}\tilde{a}_{n'} + i\sqrt{\gamma}e^{-ik|x_n|}\tilde{S}_L^+ + i\sqrt{\gamma}e^{-ik|D-x_n|}\tilde{S}_R^+, \quad (2)$$

where ω_0 is the resonant frequency, Γ, γ are the dissipative and radiative decay rates, respectively, $\Lambda_{nn'} = e^{-ik|x_n - x_{n'}|}$ with x_n being the location of the side-branch tubes ($d_n = x_{n+1} - x_n$), $k = \omega/c$ is the wave number in air with speed of sound c, and $D = Qd$ is the period of the compound unit cell. $\tilde{S}_L^+ = S_L^+ e^{i\omega t}$ and $\tilde{S}_R^+ = S_R^+ e^{i\omega t}$ correspond to the incident acoustic waves from the left and right ports, respectively. The output acoustic waves S_L^- and S_R^- are linked to the input waves by the scattering matrix,

$$\begin{pmatrix} S_L^- \\ S_R^- \end{pmatrix} = \begin{pmatrix} t & r_L \\ r_R & t \end{pmatrix}\begin{pmatrix} S_R^+ \\ S_L^+ \end{pmatrix}. \quad (3)$$

Protected by the reciprocity, the transmission coefficients in the cases of left incidence and right incidence must be the same. The transmission coefficients can be obtained by considering $S_R^+ = 0$. It reads

$$t = e^{-ikD} + i\sqrt{\gamma}\sum_{n=1}^{Q} e^{-ik(D-x_n)}\frac{a_n}{S_L^+}. \quad (4)$$

The reflection coefficients in the left incidence and right incidence cases are in general different due to the lack of mirror symmetry of the compound unit cell. The reflection coefficient for the left incidence case can be obtained with $S_R^+ = 0$ and it yields

$$r_L = i\sqrt{\gamma}\sum_{n=1}^{Q} e^{-ikx_n}\frac{a_n}{S_L^+}, \quad (5)$$

while the reflection coefficient with $S_L^+ = 0$ in the right incidence case is

$$r_R = i\sqrt{\gamma}\sum_{n=1}^{Q} e^{-ik(D-x_n)}\frac{a_n}{S_R^+}. \quad (6)$$

Band structure.—We first investigate the band structure of the acoustic system without dissipative losses, i.e., $\Gamma = 0$. The targeted frequency range is determined by the resonance frequency of the side-branch tubes, $\omega_0 \approx c\pi/l_0/2$. In the absence of modulation ($\delta = 0$), a flat band would appear at the resonance frequency of the side-branch tubes (see Supplemental Material, Note 1 [51]), which can be attributed to the strong interplay between the Bragg scattering (destructive interference of the re-radiated waves from two adjacent side-branch tubes with distance $d = \lambda_0/2$ and $\lambda_0 = 2\pi c/\omega_0$) and local resonance. The introduction of modulation ($\delta \neq 0$) forms a compound unit cell with an enlarged period (from d to $D = Qd$). Consequently, the flat band splits into Q bands due to band folding. The band structure of the compound unit cell can be calculated by using the scattering matrix $S_1 = \left(\begin{smallmatrix} t & r_L \\ r_R & t \end{smallmatrix}\right)$ and the Bloch boundary condition $S_R^- = e^{ik_B D}S_L^+$ and $S_R^+ = e^{ik_B D}S_L^-$,

$$\left| S_1 - \begin{pmatrix} e^{-ik_B D} & 0 \\ 0 & e^{ik_B D} \end{pmatrix} \right| = 0. \quad (7)$$

Figure 2(a) displays the projected band structure as a function of ϕ for a compound unit cell with $\delta = 0.4$ and $b = 1/3$, indicating that there are three side-branch tubes in a unit cell. The flat band splits into three bands (gray regions) separated by two band gaps. The Chern numbers of the three bands are obtained from the phase spectroscopy of the semi-infinite structure [52,53] (see Supplemental Material, Note 2 [51]), and are marked in Fig. 2(a). The Chern numbers, i.e., $C = 1, -2, 1$, suggest the existence of topological edge modes in the two band gaps according to the bulk-boundary correspondence developed for the Hermitian system [47–49].

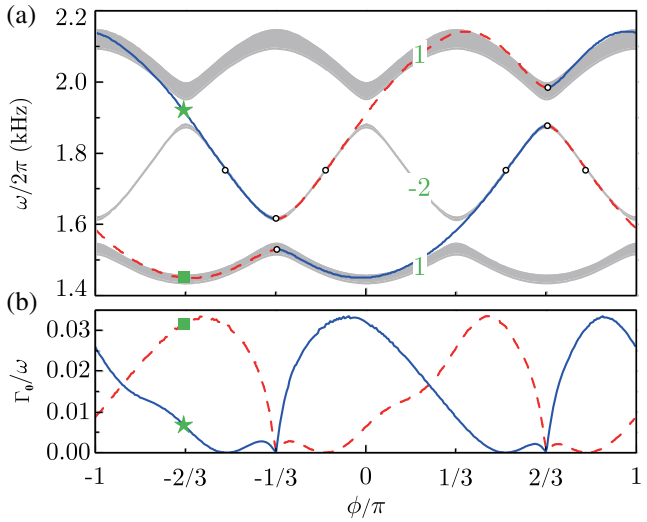

FIG. 2. (a) Projected acoustic band structure of the compound unit cell with $b = 1/3$ as a function of ϕ. The gray regions represent three pass bands separated by two band gaps. The Chern number for each pass band is marked. The eigenfrequencies of the edge modes under left (right) incidence is illustrated with blue (red dashed) line. White circles indicate the points where $\Gamma_0 = 0$. (b) The critical loss Γ_0 of the edge modes for left (blue line) and right (red dashed line) incidence. The left edge state and right edge state at $\phi = -2.1$ ($\phi/\pi = -2/3$) are marked by star and square, respectively. The parameters for the calculation are $\omega_0/2\pi = 1.75$ kHz and $\gamma/2\pi = 0.48$ kHz, which are extracted from a full wave simulation.

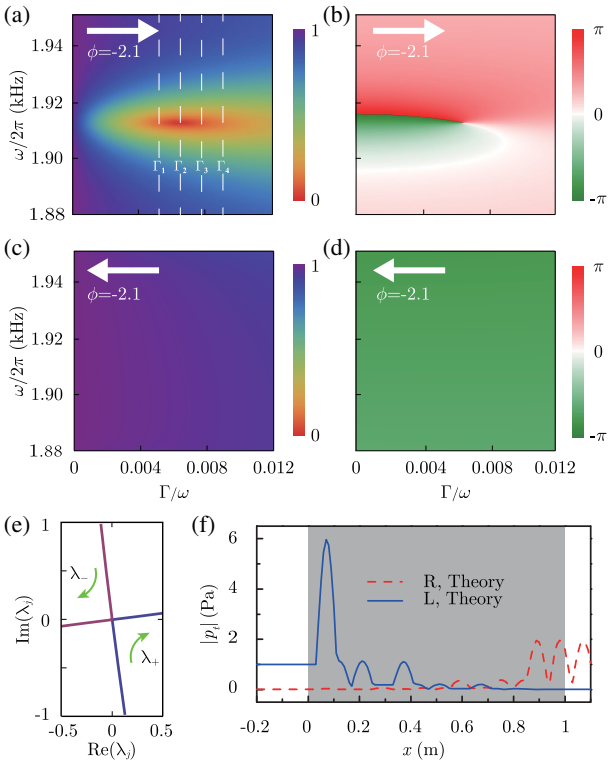

FIG. 3. The calculated reflectivity and reflection phase of the finite structure with three unit cells as a function of Γ in the second band gap with $\phi = -2.1$ (a),(b) for the left incidence and (c),(d) for the right incidence. Γ_1/ω, Γ_2/ω, Γ_3/ω, and Γ_4/ω are the loss values used in the simulation and experiment, and they are 0.0051, 0.0063, 0.0074, and 0.0086, respectively. (e) is the trajectories of eigenvalues $\lambda_\pm$ in the complex plane. The frequency is fixed at $\omega_0/2\pi = 1913$ Hz, and the variation parameter is $\Gamma/2\pi$ with value range (0, 0.012). (f) is the field distribution at the point $(\omega_0/2\pi, \Gamma_0/\omega_0) = (1913\ \text{Hz}, 0.0063)$ for left input and right input.

Topological edge states.—For a semi-infinite system, an interesting property of the topological edge mode is that the reflectivity reduces to zero with a proper amount of loss [46,54]. Therefore, the edge state can be retrieved from the zeros of the reflection coefficient, i.e., $r_\infty(\omega, \Gamma) = 0$, with critical loss $\Gamma = \Gamma_0$. We will later on show that this coincidentally links the edge state to EP. For the current structure, the zeros of $r_\infty(\omega, \Gamma)$ are identical to the zeros of $r(\omega, \Gamma)$ for a unit cell (see Supplemental Material, Note 3 [51]). The eigenfrequencies of the topological edge modes localized on the left (right) boundary can be calculated under the condition $r_L(\omega, \Gamma) = 0$ $[r_R(\omega, \Gamma) = 0]$. Edge states exist when the bands possess different Chern numbers. It is not surprising that two edge states exist for our modulated compound unit cell for any given ϕ: one for the left incidence and one for the right incidence [Fig. 2(a)]. The topological edge states connect two adjacent pass bands and part of the edge state lies in the pass band which was also observed in previous studies [30,32].

The critical loss Γ_0 for left edge state and right edge state is plotted as a function of ϕ, shown in Fig. 2(b). The points where $\Gamma_0 = 0$ are marked by circles in Fig. 2(a). Among these points, there are four of them at $\phi = -\pi/3$ and $2\pi/3$, where d_1 equals d_2, and the eigenmodes of the unit cell have symmetry and antisymmetry shapes (see Supplemental Material, Note 4 [51]). The rest of them on the left (right) edge state are located at the resonance frequency of the side-branch tube (around 1750 Hz) with $d_1 = d$ ($d_2 = d$), and the unit cell has a bound state which stems from the destructive interference of the waves from two side-branch tubes. This was recently studied and termed bound states in the continuum [55,56].

Topological edge state in a finite structure and the EP.—Next, we study the topological edge state in a finite structure composed of N unit cells with $\phi = -2.1$, where a left topological edge state lies in the second band gap marked by the green star in Fig. 2(a). The transport properties of such system can be described by the scattering matrix $S_N = \begin{pmatrix} t_N & r_{L(N)} \\ r_{R(N)} & t_N \end{pmatrix}$, which can be obtained from Eqs. (2) and (4)–(6). The main properties of the edge state, including the frequency and the critical loss Γ_0, are determined by the unit cell. In the lossless case, three unit cells are found sufficient to obtain high reflectivity (band gap). The reflectivity of three unit cells for left input is calculated as a function of ω (in the second band gap

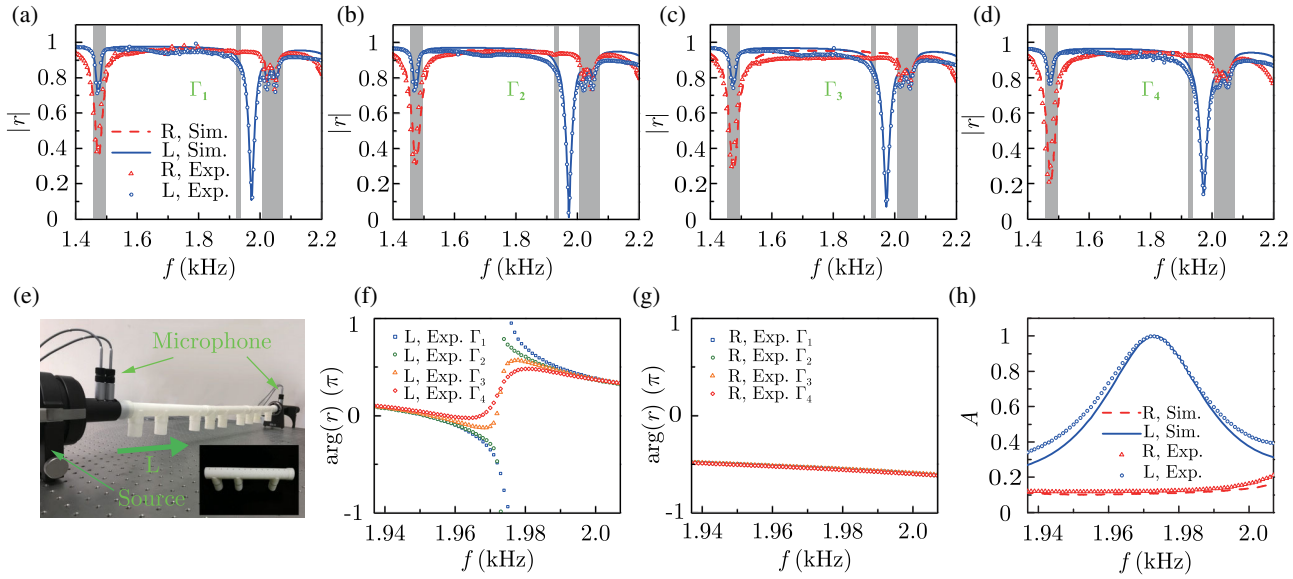

FIG. 4. Simulated and measured reflectivity and reflection phase of the finite structure with three unit cells and different losses Γ_1, Γ_2, Γ_3, and Γ_4. (a)–(d) refer to the reflectivity for Γ_1, Γ_2, Γ_3, and Γ_4, respectively. The three gray regions represent the pass bands. (e) The experimental setup. The inset figure is one unit cell of the sample and the small side holes are used to measure the field distribution. The measured reflection phases at different losses (f) for left incidence and (g) for right incidence. (h) The simulated and measured sound absorption at frequencies in the second band gap where $\Gamma = \Gamma_2$. The blue solid lines (red dashed lines) are the simulated results for left incidence (right incidence). The blue open circles (red open triangles) are the experimental results for left incidence (right incidence).

frequency range) and Γ, as shown in Fig. 3(a). A zero reflectivity is seen at the point $(\omega_0/2\pi, \Gamma_0/\omega_0) = (1913\ \text{Hz}, 0.0063)$, which is the EP. The pressure field distribution for this point with waves coming from the left side is calculated and shown in Fig. 3(f). The field is significantly enhanced at the left edge, confirming the existence of the edge state.

The eigenvalues $\lambda_\pm = t_N \pm \sqrt{r_{L(N)} r_{R(N)}}$ of the scattering matrix are calculated with the frequency $\omega_0/2\pi = 1913$ Hz. Their trajectories [25] in the complex plane are shown in Fig. 3(e). The real parts of the two eigenvalues are anticrossing and their imaginary parts are crossing, which are the characteristics of EPs [24]. At the EP where $\Gamma/2\pi$ equals 0.0063, the two eigenvalues $\lambda_\pm$ and their corresponding eigenvectors $\begin{pmatrix} \pm\sqrt{r_{L(N)}/r_{R(N)}} \\ 1 \end{pmatrix}$ coalesce. The phase of the reflected wave for left input is also shown in Fig. 3(b), and a vortex-like pattern centered at the EP is noted. For the edge state locked on the left side at this particular point, extremely asymmetric transport is achieved. The reflectivity and the reflection phase for the right input case shown in Figs. 3(c) and 3(d) remain almost unchanged in the parameter space. The reflectivity remains almost unity for ω within the band gap. Figure 3(e) suggests that the two eigenvalues are zero at the EP, which indicate perfect absorption with specific inputs [57]. For our case, the eigenvector is $\binom{0}{1}$, corresponding to the left input only, and consequently unidirectional perfect absorption state (UPA) can be established. The UPA state can be obtained as long as the edge state is located in the band gap and the finite structure is sufficiently long, so that the transmission t_N can be regarded as zero.

To confirm our theory, a series of acoustic experiments are conducted to measure the reflection coefficients of a sample composed of three unit cells with four different loss values corresponding to Γ_1, Γ_2 (critical loss), Γ_3, and Γ_4 in Fig. 3(a). The experimental setup for the left incidence case is shown in Fig. 4(e). For the right incidence case, we simply reverse the sample. The acoustic energy loss is introduced by sponges. The loss value is adjusted and extracted using methods described in Supplemental Material, Note 5 [51]. The measured results on the reflectivity are shown in Figs. 4(a)–4(d) for Γ_1, Γ_2, Γ_3, and Γ_4, respectively. It is seen that the reflectivity for the left input case at 1973 Hz (this frequency is slightly different from the theoretically predicted one, i.e., 1913 Hz) decreases first from Γ_1 to Γ_2 and then increases from Γ_2 to Γ_3, and to Γ_4. It is also observed that the reflectivity for the right input wave is almost unity in the second band gap. A series of simulations using COMSOL Multiphysics are performed to corroborate the measurement. These results are shown by lines in Figs. 4(a)–4(d), where excellent agreements can be observed. In addition to the left edge state located in the second band gap, a right edge state located in the first pass band also exists when $\phi = -2.1$. A brief discussion on this edge state can be found in Supplemental Material, Note 6 [51].

The measured reflection phases in the second band gap for different losses are shown in Fig. 4(f) for left incidence

and in Fig. 4(g) for right incidence. The left reflection phase has a dramatic transition from $-\pi$ to π for a lower loss with Γ_1, which is the characteristic of the Lorentz resonance. When the loss is greater than the critical loss Γ_0, the reflection phase changes smoothly for the cases of Γ_3 and Γ_4. Meanwhile, the right incidence reflection phase remains almost unchanged with different losses as shown in Fig. 4(g). Besides, the measured and simulated sound absorption coefficients defined by $A = 1 - |t|^2 - |r|^2$ in the second band gap frequency range for $\Gamma = \Gamma_2$ are plotted in Fig. 4(h). The absorption at 1973 Hz is almost perfect for the left incident wave and is significantly weaker when the incoming wave is from the other direction. Finally, the internal pressure field at 1973 Hz with loss $\Gamma = \Gamma_2$ is measured to confirm the existence of the edge state mode. The results can be found in the Supplemental Material, Note 7 [51].

Conclusion.—The comblike, quasiperiodic acoustic structures with compound unit cells provide us a platform to study the topologically protected edge states in an open and non-Hermitian system. The EP is obtained by tailoring the intrinsic loss. The URP/UPA and topologically protected edge states are simultaneously observed. Our theory is generic to wave physics and can be readily extended to photonics and plasmonics. Our work provides a new route to studying the connection between topological edge state, non-Hermitian physics, and exceptional point.

This work was supported by the National Key Research Program of China (Grant No. 2016YFA0301101), the National Natural Science Foundation of China (Grants No. 11704284, No. 11775159, No. 61621001, and No. 11674247), Shanghai Science and Technology Committee (Grant No. 18JC1410900), and Shanghai Pujiang Program under Grant No. 17PJ1409000. Y. L. acknowledges the start-up funds from Tongji University.

*yongli@tongji.edu.cn
†yjing2@ncsu.edu
‡hongchen@tongji.edu.cn

[1] C. M. Bender, S. Boettcher, and P. N. Meisinger, J. Math. Phys. (N.Y.) **40**, 2201 (1999).
[2] A. Guo, G. J. Salamo, D. Duchesne, R. Morandotti, M. Volatier-Ravat, V. Aimez, G. A. Siviloglou, and D. N. Christodoulides, Phys. Rev. Lett. **103**, 093902 (2009).
[3] K. G. Makris, R. El-Ganainy, D. N. Christodoulides, and Z. H. Musslimani, Phys. Rev. Lett. **100**, 103904 (2008).
[4] Z. Lin, H. Ramezani, T. Eichelkraut, T. Kottos, H. Cao, and D. N. Christodoulides, Phys. Rev. Lett. **106**, 213901 (2011).
[5] B. Peng, Ş. K. Özdemir, F. Lei, F. Monifi, M. Gianfreda, G. L. Long, S. Fan, F. Nori, C. M. Bender, and L. Yang, Nat. Phys. **10**, 394 (2014).
[6] X. Zhu, H. Ramezani, C. Shi, J. Zhu, and X. Zhang, Phys. Rev. X **4**, 031042 (2014).
[7] H. Hodaei, M. A. Miri, M. Heinrich, D. N. Christodoulides, and M. Khajavikhan, Science **346**, 975 (2014).
[8] L. Feng, Z. J. Wong, R. M. Ma, Y. Wang, and X. Zhang, Science **346**, 972 (2014).
[9] A. Regensburger, C. Bersch, M. A. Miri, G. Onishchukov, D. N. Christodoulides, and U. Peschel, Nature (London) **488**, 167 (2012).
[10] Y. Sun, W. Tan, H. Q. Li, J. Li, and H. Chen, Phys. Rev. Lett. **112**, 143903 (2014).
[11] R. Fleury, D. Sounas, and A. Alu, Nat. Commun. **6**, 5905 (2015).
[12] C. Shi, M. Dubois, Y. Chen, L. Cheng, H. Ramezani, Y. Wang, and X. Zhang, Nat. Commun. **7**, 11110 (2016).
[13] Y. Auregan and V. Pagneux, Phys. Rev. Lett. **118**, 174301 (2017).
[14] T. Liu, X. Zhu, F. Chen, S. Liang, and J. Zhu, Phys. Rev. Lett. **120**, 124502 (2018).
[15] C. Dembowski, H. D. Graf, H. L. Harney, A. Heine, W. D. Heiss, H. Rehfeld, and A. Richter, Phys. Rev. Lett. **86**, 787 (2001).
[16] S. B. Lee, J. Yang, S. Moon, S. Y. Lee, J. B. Shim, S. W. Kim, J. H. Lee, and K. An, Phys. Rev. Lett. **103**, 134101 (2009).
[17] B. Zhen, C. W. Hsu, Y. Igarashi, L. Lu, I. Kaminer, A. Pick, S. L. Chua, J. D. Joannopoulos, and M. Soljačić, Nature (London) **525**, 354 (2015).
[18] K. Ding, G. Ma, M. Xiao, Z. Q. Zhang, and C. T. Chan, Phys. Rev. X **6**, 021007 (2016).
[19] J. Wiersig, Phys. Rev. Lett. **112**, 203901 (2014).
[20] H. Hodaei, A. U. Hassan, S. Wittek, H. Garcia-Gracia, R. El-Ganainy, D. N. Christodoulides, and M. Khajavikhan, Nature (London) **548**, 187 (2017).
[21] W. Chen, S. K. Ozdemir, G. Zhao, J. Wiersig, and L. Yang, Nature (London) **548**, 192 (2017).
[22] L. Feng, Y. L. Xu, W. S. Fegadolli, M. H. Lu, J. E. Oliveira, V. R. Almeida, Y. F. Chen, and A. Scherer, Nat. Mater. **12**, 108 (2013).
[23] L. Feng, X. Zhu, S. Yang, H. Zhu, P. Zhang, X. Yin, Y. Wang, and X. Zhang, Opt. Express **22**, 1760 (2014).
[24] Y. Huang, G. Veronis, and C. Min, Opt. Express **23**, 29882 (2015).
[25] J. Gear, Y. Sun, S. Xiao, L. Zhang, R. Fitzgerald, S. Rotter, H. Chen, and J. Li, New J. Phys. **19**, 123041 (2017).
[26] M. Z. Hasan and C. L. Kane, Rev. Mod. Phys. **82**, 3045 (2010).
[27] X. L. Qi and S. C. Zhang, Rev. Mod. Phys. **83**, 1057 (2011).
[28] F. D. M. Haldane and S. Raghu, Phys. Rev. Lett. **100**, 013904 (2008).
[29] Z. Wang, Y. D. Chong, J. D. Joannopoulos, and M. Soljačić, Phys. Rev. Lett. **100**, 013905 (2008).
[30] K. Fang, Z. Yu, and S. Fan, Nat. Photonics **6**, 782 (2012).
[31] M. Hafezi, S. Mittal, J. Fan, A. Migdall, and J. M. Taylor, Nat. Photonics **7**, 1001 (2013).
[32] A. B. Khanikaev, S. H. Mousavi, W. K. Tse, M. Kargarian, A. H. MacDonald, and G. Shvets, Nat. Mater. **12**, 233 (2013).
[33] T. Ma, A. B. Khanikaev, S. H. Mousavi, and G. Shvets, Phys. Rev. Lett. **114**, 127401 (2015).
[34] L. H. Wu and X. Hu, Phys. Rev. Lett. **114**, 223901 (2015).

[35] M. Xiao, G. Ma, Z. Yang, P. Sheng, Z. Q. Zhang, and C. T. Chan, Nat. Phys. **11**, 240 (2015).
[36] C. He, X. Ni, H. Ge, X.-C. Sun, Y.-B. Chen, M.-H. Lu, X.-P. Liu, and Y.-F. Chen, Nat. Phys. **12**, 1124 (2016).
[37] J. Lu, C. Qiu, L. Ye, X. Fan, M. Ke, F. Zhang, and Z. Liu, Nat. Phys. **13**, 369 (2017).
[38] Y. G. Peng, C. Z. Qin, D. G. Zhao, Y. X. Shen, X. Y. Xu, M. Bao, H. Jia, and X. F. Zhu, Nat. Commun. **7**, 13368 (2016).
[39] Y. Deng, H. Ge, Y. Tian, M. Lu, and Y. Jing, Phys. Rev. B **96**, 184305 (2017).
[40] J. M. Zeuner, M. C. Rechtsman, Y. Plotnik, Y. Lumer, S. Nolte, M. S. Rudner, M. Segev, and A. Szameit, Phys. Rev. Lett. **115**, 040402 (2015).
[41] C. Poli, M. Bellec, U. Kuhl, F. Mortessagne, and H. Schomerus, Nat. Commun. **6**, 6710 (2015).
[42] S. Weimann, M. Kremer, Y. Plotnik, Y. Lumer, S. Nolte, K. G. Makris, M. Segev, M. C. Rechtsman, and A. Szameit, Nat. Mater. **16**, 433 (2017).
[43] L. Xiao, X. Zhan, Z. H. Bian, K. K. Wang, X. Zhang, X. P. Wang, J. Li, K. Mochizuki, D. Kim, N. Kawakami, W. Yi, H. Obuse, B. C. Sanders, and P. Xue, Nat. Phys. **13**, 1117 (2017).
[44] M. A. Bandres, S. Wittek, G. Harari, M. Parto, J. Ren, M. Segev, D. N. Christodoulides, and M. Khajavikhan, Science **359**, eaar4005 (2018).
[45] H. Y. Zhou, C. Peng, Y. Yoon, C. W. Hsu, K. A. Nelson, L. Fu, J. D. Joannopoulos, M. Soljačić, and B. Zhen, Science **359**, 1009 (2018).
[46] A. V. Poshakinskiy, A. N. Poddubny, L. Pilozzi, and E. L. Ivchenko, Phys. Rev. Lett. **112**, 107403 (2014).
[47] L. J. Lang, X. Cai, and S. Chen, Phys. Rev. Lett. **108**, 220401 (2012).
[48] Y. E. Kraus and O. Zilberberg, Phys. Rev. Lett. **109**, 116404 (2012).
[49] Y. E. Kraus, Y. Lahini, Z. Ringel, M. Verbin, and O. Zilberberg, Phys. Rev. Lett. **109**, 106402 (2012).
[50] S. H. Fan, W. Suh, and J. D. Joannopoulos, J. Opt. Soc. Am. A **20**, 569 (2003).
[51] See Supplemental Material at http://link.aps.org/supplemental/10.1103/PhysRevLett.121.124501 for details on the functionality of modulation, Chern number of bulk bands, the interpretation of topological edge states, the method of tuning losses with sponges, etc.
[52] A. V. Poshakinskiy, A. N. Poddubny, and M. Hafezi, Phys. Rev. A **91**, 043830 (2015).
[53] C. Caloz and T. Itoh, *Electromagnetic Metamaterials: Transmission Line Theory and Microwave Applications* (Wiley, Hoboken, NJ, 2006).
[54] K. Y. Bliokh, Y. P. Bliokh, V. Freilikher, S. Savelev, and F. Nori, Rev. Mod. Phys. **80**, 1201 (2008).
[55] C. W. Hsu, B. Zhen, A. D. Stone, J. D. Joannopoulos, and M. Soljačić, Nat. Rev. Mater. **1**, 16048 (2016).
[56] Y. X. Xiao, G. Ma, Z. Q. Zhang, and C. T. Chan, Phys. Rev. Lett. **118**, 166803 (2017).
[57] Y. D. Chong, L. Ge, H. Cao, and A. D. Stone, Phys. Rev. Lett. **105**, 053901 (2010).